THE JOURNAL OF PHYSICAL CHEMISTRY C

pubs.acs.org/JPCC Article

Zipper-Like Unfolding of dsDNA Caused by Graphene Wrinkles

Baoyu Li, Yuanzhao Zhang, Xuan-Yu Meng,* and Ruhong Zhou*

Cite This: J. Phys. Chem. C 2020, 124, 3332−3340 Read Online

ACCESS | Metrics & More | Article Recommendations | Supporting Information

ABSTRACT: Wrinkles have been frequently observed in a graphene nanosheet. Such structural corrugations can influence graphene's characteristics and have received considerable attention recently. However, the impact of these wrinkles on the critical graphene interactions with biomolecules remains unclear. Here, we investigate the interaction of a double-stranded DNA (dsDNA) segment with a wrinkled graphene nanosheet using molecular dynamics simulations. We find that dsDNA experiences severe structural deformation upon binding to a wrinkled graphene surface, whereas it tends to maintain its native structure upon binding to an idealized graphene nanosheet. Further analysis reveals that it is energetically advantageous for the terminal bases to bind to the wrinkled area, serving as anchors on the nanosheet. Consequently, movement of the remaining part of the dsDNA generates a "centripetal stretching" force to the anchoring bases, causing the breakage of the interbase hydrogen bonds and local unfolding. Like a slider opening up a zipper, the local unfolding proceeds sequentially from the first base pair to the next until the end. This zipper-like unfolding subsequently exposes more DNA bases to contact with the wrinkled area, thus accelerating the dsDNA deformation. These findings highlight the importance of wrinkles in the interaction of graphene with biomolecules and deepen our understanding of graphene nanotoxicity in general.

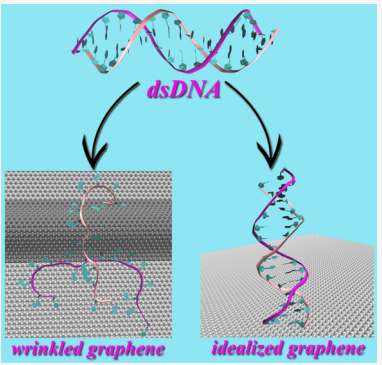

INTRODUCTION

Graphene, a two-dimensional material made of a honeycomb carbon lattice, has a number of extraordinary electrical, optical, thermal, and mechanical properties.[1−6] It has been widely adopted for various applications, including transparent conductors, energy-storage batteries, and nanoelectronic devices.[7−11] Graphene-based nanomaterials are especially promising for biomedical applications, with potential for use in drug and gene delivery, cell and tumor imaging, as well as cancer photothermal therapy.[12−17] Additionally, it has been reported that graphene can be used as a biosensor to detect various biomolecules and as a substrate to control the growth, differentiation, and functions of specific types of cells.[7−11,18−21]

Despite these promising progresses, there have been increasing concerns on the potential nanotoxicity of graphene-based nanomaterials when coming into contact with biological organisms. For instance, nanomaterials can be inhaled and accumulate in the cytoplasm, which may lead to lung injury, immunologic impairment, and adverse cardiovascular effects.[22−26] A recent study indicates that nanomaterials can compromise the structural integrity of cell membranes by extracting large amounts of phospholipids, which in turn results in cell death.[27] Moreover, a number of studies have found that nanomaterials can induce severe distortions of biomolecules due to their strong hydrophobic interactions.[28−30] The interactions of nucleic acids with ideal two-dimensional nanomaterial surfaces (e.g., hexagonal boron nitride, palladium, nitrogenized graphene (C_2N), graphene, carbon nanotubes (CNTs), molybdenum disulfide (MoS_2), and tungsten disulfide (WS_2)) have been widely studied.[31−35] In addition, several studies have been conducted using both theoretical and experimental methods to investigate how a force induces changes in the structure of nucleic acids at the atomic level.[36−40] We have also previously studied DNA interactions with nanomaterials using both experimental and theoretical approaches. For instance, we characterized the binding patterns and dynamics of a small double-stranded DNA (dsDNA) segment on the recently synthesized C_2N and found that the dsDNA repeatedly exhibits a strong preference in its binding mode on the C_2N substrate, displaying an upright orientation that is independent of its initial configurations.[32] When compared to graphene, C_2N was also found to show a milder attraction to dsDNA, which was confirmed by experiments.[32] In another recent study,[41] we used both surface-enhanced Raman scattering spectra and molecular dynamics (MD) simulations to study single-stranded DNA (ssDNA)-anchored gold nanoparticles (AuNPs), which revealed that single-nanoparticle-layer plasmonic films made of these ssDNA−AuNPs display a rapid and reversible red−blue color change upon the wetting−dewetting transition, suggesting a hydration-induced microscopic plasmonic coupling between ssDNA and AuNPs.[41] We have also

Received: September 16, 2019
Revised: January 9, 2020
Published: January 10, 2020

https://dx.doi.org/10.1021/acs.jpcc.9b08778
J. Phys. Chem. C 2020, 124, 3332−3340

combined MD simulations with electrochemical experiments to explore the dynamics of ssDNA immobilized on high-curvature versus flat surfaces of gold nanostructures and found that high-curvature structures suppress DNA probe aggregation among adjacent probes, resulting in conformations that are more freely accessed by target molecules.[42] The effect was further amplified in the presence of highly charged cations commonly used in electrochemical biosensing.[42]

Meanwhile, wrinkles are ubiquitous in graphene sheets and are hard to avoid for graphene prepared either by chemical vapor deposition or by micromechanical exfoliation.[43−45] Such structural corrugations can significantly alter graphene's material properties. For example, the local strain redistribution and π-cloud rehybridization caused by these wrinkles can modify the electrical properties of graphene, with potential applications in graphene-based electronics, bioelectronics, and self-assembly of complex structures.[46−49] Moreover, wrinkles of a certain size can induce a magnetic field and lead to the formation of a zero-energy Landau level.[50] On the other hand, when applied as a scaffold to attach nanoparticles, wrinkled graphene can also be used to store energy.[51] However, to the best of our knowledge, the effect of wrinkles on the interaction of graphene with biomolecules is still unknown. Many previous studies have indicated that the morphology of nanomaterials can influence their biological performances such as cellular uptake, biodistribution, blood circulation duration, and excretion.[52−54] With the increasing adoption of graphene-based nanomaterials in biomedical applications, it has become even more urgent to understand how wrinkles affect graphene−biomolecule interactions, especially given the recently discovered potential toxicity of graphene.[27,29,30,55]

In this work, using molecular dynamics (MD) simulations, we investigate the interaction between a wrinkled graphene (W-Gra) nanosheet and a model double-stranded DNA (dsDNA) segment (5′ → 3′ single-strand sequence: ATCGATCGATCGATCG). For comparison, we also simulate the interaction of the dsDNA segment with an idealized graphene (I-Gra) nanosheet. Our results show that the dsDNA can be attracted to and bound on both W-Gra and I-Gra. However, behaviors of dsDNA on the two graphene surfaces are different: upon binding to I-Gra, the dsDNA's native structure is well preserved apart from minimal denaturation at the terminal. In contrast, the dsDNA experiences severe structural deformation after binding to the W-Gra surface. Further analysis of the free energy profile suggests a stronger binding affinity between nucleobases and the wrinkled area than that between nucleobases and the planar area. Upon binding to the W-Gra nanosheet, it is energetically favorable for the contacting bases to bind to the wrinkled area, which highly restrains the mobility of these bases and causes them to act like "anchors". The large motions of other parts of dsDNA create a "centripetal stretching" force to those anchoring bases, causing the breakage of hydrogen bonds between the base pairs. Then, the zipper-like unfolding process exposes more DNA base pairs to be in contact with the W-Gra surface via a strong $\pi-\pi$ stacking interaction, which in turn leads to more severe structural deformation. These findings not only elucidate the important role of wrinkles at the nano−bio interface but also provide deeper insight into graphene nanotoxicity in general.

SIMULATION METHODS

All-Atom MD Simulations. The W-Gra nanosheet used in our simulations consists of 3600 carbon atoms with a dimension of 9.89 nm × 8.80 nm, while the I-Gra nanosheet consists of 2800 carbon atoms with a dimension of 8.60 nm × 8.51 nm. The carbon atoms in both W-Gra and I-Gra nanosheets were modeled as uncharged Lennard−Jones particles with a cross section of σ_{cc} = 0.34 nm and a potential well depth of ε_{cc} = 0.36 kJ/mol.[56,57] The B-form dsDNA model (5′ → 3′ single-strand sequence: ATCGATCGATCGATCG) was generated from the http://structure.usc.edu/make-na/server.html server and modeled with the CHARMM27 force field.[58] To further improve the reliability of our simulations, the adsorption of dsDNA on W-Gra was also simulated using the CHARMM36[59] and AMBER03 force field,[60] respectively. As shown in Figure 1, the dsDNA was initially placed above

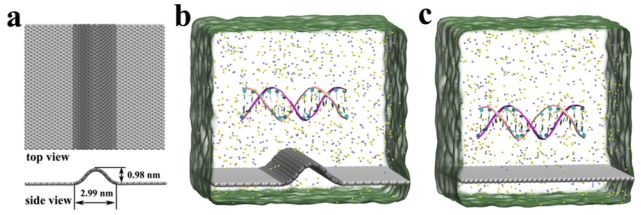

Figure 1. (a) Top and side views of the W-Gra nanosheet. Carbon atoms in the wrinkled area are shown as gray spheres, while others are shown as silver spheres. The dimension of the wrinkle is labeled in the side view. The dsDNA is placed directly above the W-Gra (b) and I-Gra (c) nanosheets in the initial systems. The dsDNA is shown in the ribbon representation with the backbone of each chain colored differently (chain A, pink; chain B, purple). K^+ and Cl^- ions are displayed as blue and yellow spheres, respectively. Water is not shown, except at the boundaries.

each of the graphene sheets with a minimum distance of 1.63 nm. Following similar protocols used in our previous studies,[61−64] the combined systems were then solvated in a cubic water box with periodic boundary conditions in all three dimensions, with atoms in W-Gra and I-Gra nanosheets fixed during all simulations. The TIP3P water model[65] was used for water molecules. K^+ and Cl^- ions were added to neutralize the entire system, yielding a 1 M KCl electrolyte. The detailed information of the two systems is summarized in Table 1.

Table 1. Information for the Two Systems Simulated in This Work

	dsDNA—W-Gra	dsDNA—I-Gra
box size (nm^3)	9.89 × 8.80 × 9.00	8.60 × 8.51 × 9.00
number of water molecules	23 150	19 440
number of ions	502 K^+ and 472 Cl^-	427 K^+ and 397 Cl^-
total number of atoms	75 038	62 958

The simulations were carried out with the GROMACS software package.[66] The VMD software[67] was used to analyze and visualize the trajectory data. The van der Waals (vdW) interactions were handled with a smooth cutoff of 1.0 nm, whereas the particle mesh Ewald method[68,69] (using a fourth-order interpolation and a maximum Fourier spacing of 0.1 nm) was used to treat the long-range Coulomb interactions. Covalent bond lengths involving hydrogen atoms were constrained using the LINCS algorithm.[70] After energy

https://dx.doi.org/10.1021/acs.jpcc.9b08778
J. Phys. Chem. C 2020, 124, 3332−3340

minimization, all simulations were equilibrated for 0.5 ns in the NVT ensemble using the v-rescale thermostat[71] at 300 K. After that, the systems were further equilibrated in the NPT ensemble for another 0.5 ns under a constant pressure of 1 bar and a temperature of 300 K, implemented through the Berendsen coupling method.[72] During the NVT and NPT equilibrium processes, all heavy atoms in dsDNA were harmonically constrained with a force constant of 1000 kJ/mol/nm^2. For each system, three independent trajectories of 1.5 μs in duration were generated, yielding a total simulation time of 9 μs. The integration time step was 2 fs, and data were collected every 2 ps for analysis.

Potential of Mean Force (PMF) Profile. The potential of mean force (PMF) of a representative base (Adenine) along the z-direction of the wrinkled and planar graphene was calculated using the umbrella sampling method.[73−75] The distance (d) to its binding site was restrained at a reference distance (d_0) with a harmonic force $F = k \times (d - d_0)$, where k = 2000 kJ mol^{-1} nm^{-2} is the force constant. The spacing of the sampling windows was set to 0.05 nm. For each d_0, the systems were equilibrated for 2 ns before a 10 ns production run. The free energy profiles were obtained by the g_wham tool that implements the Weighted Histogram Analysis Method.[76]

RESULTS AND DISCUSSION

In our simulations, we found that both W-Gra and I-Gra can attract and adsorb dsDNA to form stable binding configurations. Notably, the final binding configurations of dsDNA on the W-Gra and I-Gra surfaces were remarkably distinct. As shown in Figure 2a−c, after binding to W-Gra, dsDNA

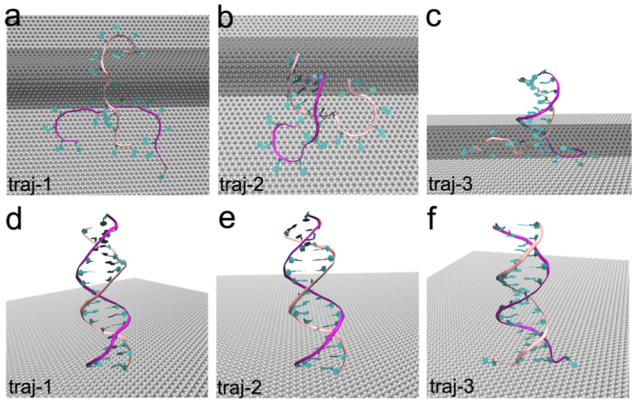

Figure 2. Final binding configurations of dsDNA when adsorbed onto W-Gra (a−c) and I-Gra (d−f) surfaces, obtained from six independent 1.5 μs trajectories. The graphene nanosheets are rotated for a better view of the dsDNA with (a), (b) parallel to the page and the rest perpendicular to the page. The color scheme is the same as in Figure 1.

experienced severe structural deformation and lost its helical structure, accompanied by the exposure of its nucleobases to the W-Gra surface. In contrast, after binding to I-Gra, the dsDNA managed to maintain its native structure (only in trajectory 3 did it show slight local unwinding at the contacting terminal). Moreover, it adopted similar binding modes in all three independent trajectories. As shown in Figure 2d−f, dsDNA ended up standing upright on the I-Gra surface, with its backbone nearly perpendicular to the nanosheet, which is similar to a previous study of the adsorption of dsDNA on C_2N.[32] Compared with I-Gra, the drastic dsDNA denaturation observed on W-Gra indicates a potential destructive effect on the graphene−biomolecule interactions caused by the surface wrinkles of the nanomaterial.

Figure 3 displays the representative snapshots from trajectory 1 of the W-Gra system, showing the adsorption kinetics of dsDNA to the W-Gra surface. The dsDNA diffused freely in bulk water for several nanoseconds before it established initial contact with W-Gra through the terminal nucleobases at t = 11 ns (Figure 3a). The initial contact was formed between terminal base A1 and the planar area of the graphene through a strong $\pi-\pi$ stacking interaction, which is common between biomolecules and carbon-based nanomaterials.[55,77,78] For t = 11−14 ns, A1 quickly slid toward the graphene wrinkle, breaking the hydrogen bonds between bases A1 and T32 (Figure 3b). Note that the movement of base A1 was highly restrained after binding to the wrinkled area, acting as an "anchor" for dsDNA (more below). The thermal motion of the other parts of dsDNA generates a centripetal stretching force to the anchoring bases A1 and T32, which caused the breakage of the neighboring hydrogen bonds between bases T2 and A31. The released bases then formed a stable $\pi-\pi$ stacking interaction with the W-Gra surface, as shown in Figure 3c,d. After that, T2 and A31 moved to the wrinkled area and were restrained there, serving as a new anchor. This process then repeats; essentially, the strong interaction from the wrinkles exposed previously distant and untouching dsDNA bases to be in contact with the W-Gra nanosheet one by one. Like a slider opening up a zipper, the local unfolding precedes sequentially from the first base pair to the next until the end. This zipper-like unfolding process continued until the dsDNA completely unfolded at around t = ∼800 ns, as depicted in Figure 3g. The representative snapshots of the adsorption process of dsDNA to W-Gra from the other two trajectories are displayed in Figures S1 and S2, which show similar unfolding processes (just Traj-3 displaying an incomplete denatured structure at the end of the current simulation length).

To further characterize the adsorption process of dsDNA on graphene nanosheets, we calculate the contact number N_{cont} between the heavy atoms of dsDNA and W-Gra/I-Gra. The results are summarized in Figure 4a. Here, a heavy atom is considered to be in contact with the nanosheet if its distance to any of the carbon atoms in the nanosheet is less than 0.5 nm. We found that the N_{cont} values in the W-Gra system are much higher than those in the I-Gra system. This is consistent with the fact that the dsDNA in the W-Gra system lost its structural integrity and bound tightly onto the wrinkled surface, while the dsDNA in the I-Gra system remained largely folded and stood upright on the surface. For the three trajectories from the W-Gra system, N_{cont} reached 100 within tens of nanoseconds and eventually grew to ∼400, ∼250, and ∼180, respectively. The jump of N_{cont} in trajectory 1 at t = 790 ns was caused by the separation of the two chains in dsDNA (see Figure 3f−h). For the I-Gra system, the N_{cont} values plateaued around 30 within tens of nanoseconds and remained there (except for a slight increase at t = 315 ns in trajectory 3 due to the breakage of the terminal base pair), indicating that dsDNA can largely maintain its native structure upon binding to the I-Gra nanosheet.

To understand the energetics of the above binding processes, we calculated the interaction energy between dsDNA and the two graphene nanosheets. The results are summarized in Figure 4b. The interaction energies of dsDNA with W-Gra are much lower than those with I-Gra, suggesting a

https://dx.doi.org/10.1021/acs.jpcc.9b08778
J. Phys. Chem. C 2020, 124, 3332−3340

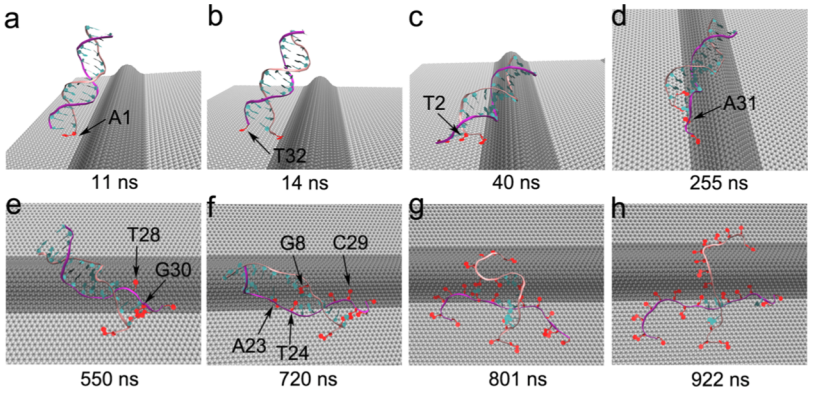

Figure 3. Representative snapshots from trajectory 1 of the W-Gra system showing the adsorption process of dsDNA onto the W-Gra surface. The bases bound to W-Gra are highlighted in red. The color codes are the same as those in Figure 1.

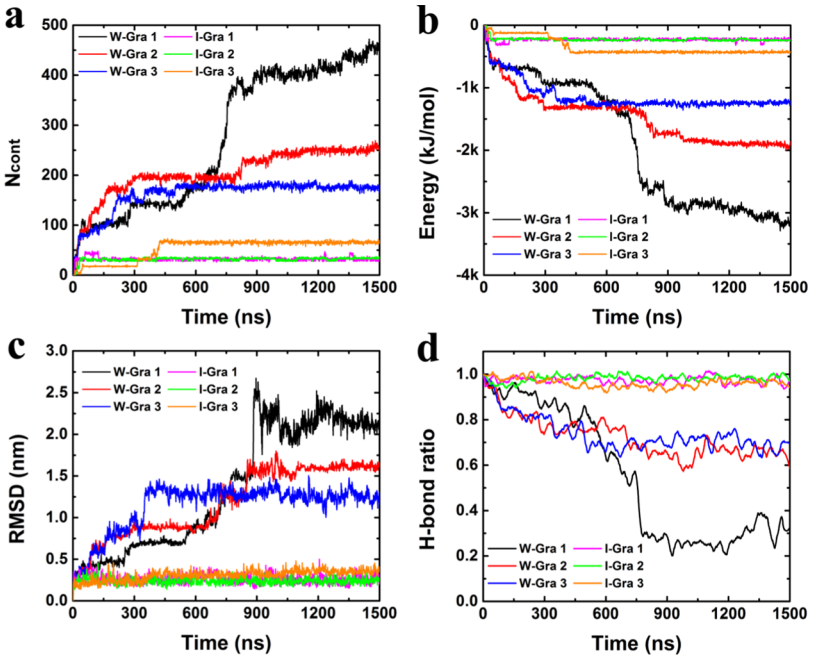

Figure 4. (a) Time-resolved contact number between dsDNA heavy atoms and W-Gra/I-Gra for six different trajectories (three for each system). (b) Interaction energies between dsDNA and W-Gra/I-Gra as a function of simulation time for the same trajectories. (c) Time evolution of the root-mean-squared deviation (RMSD) of dsDNA heavy atoms relative to the crystal structure upon binding to the W-Gra and I-Gra surfaces. (d) Ratio of the hydrogen bonds in dsDNA that remains intact upon binding to W-Gra or I-Gra as a function of simulation time.

stronger interaction between dsDNA and W-Gra. This is consistent with the values reflected in the contact number N_{cont} since more contacts usually lead to stronger interactions.

Another important indicator of the structural integrity of a biomolecule is the root-mean-squared deviation (RMSD) with respect to its native structure based on the heavy atoms. As shown in Figure 4c, for the three trajectories of the I-Gra system, the RMSDs plateaued within tens of nanoseconds and remained well below 0.4 nm. In contrast, the RMSD values for the W-Gra system kept increasing for hundreds of nanoseconds after the initial contact and all stabilized well above 1 nm.

It is well known that the internal hydrogen bonds are crucial for dsDNA to maintain its native structure. We thus calculated the fraction of interacting hydrogen bonds associated with the bases in dsDNA (defined as the number of the remaining hydrogen bonds in dsDNA divided by the number of hydrogen bonds in dsDNA at t = 0 ns) as a function of time. Here, a hydrogen bond is considered intact if the distance between the proton donor and acceptor atoms is less than 0.35 nm and the H-donor−acceptor angle is less than 30°. As shown in Figure 4d, dsDNA in the I-Gra system maintained over 90% of its hydrogen bonds for all time t, while it lost ∼70, ∼40, and ∼30% of its hydrogen bonds in the W-Gra system. This again confirms that W-Gra can cause much more severe damage to dsDNA than I-Gra.

As shown in the previous studies,[79,80] the interlayer water can play a significant role in regulating the interactions between biomolecules and nanomaterials due to some strong effects such as nanoscale dewetting.[81] We studied the water distribution around DNA bases to show the effect of the interlayer water in regulating the interactions with graphene, and the results are shown in Figure S3. We highlighted the representative base A1 for illustration. The water population in the first solvation shell of base A1 was noticeably affected once in contact with the graphene. For base A1 in bulk, there were

https://dx.doi.org/10.1021/acs.jpcc.9b08778
J. Phys. Chem. C 2020, 124, 3332−3340

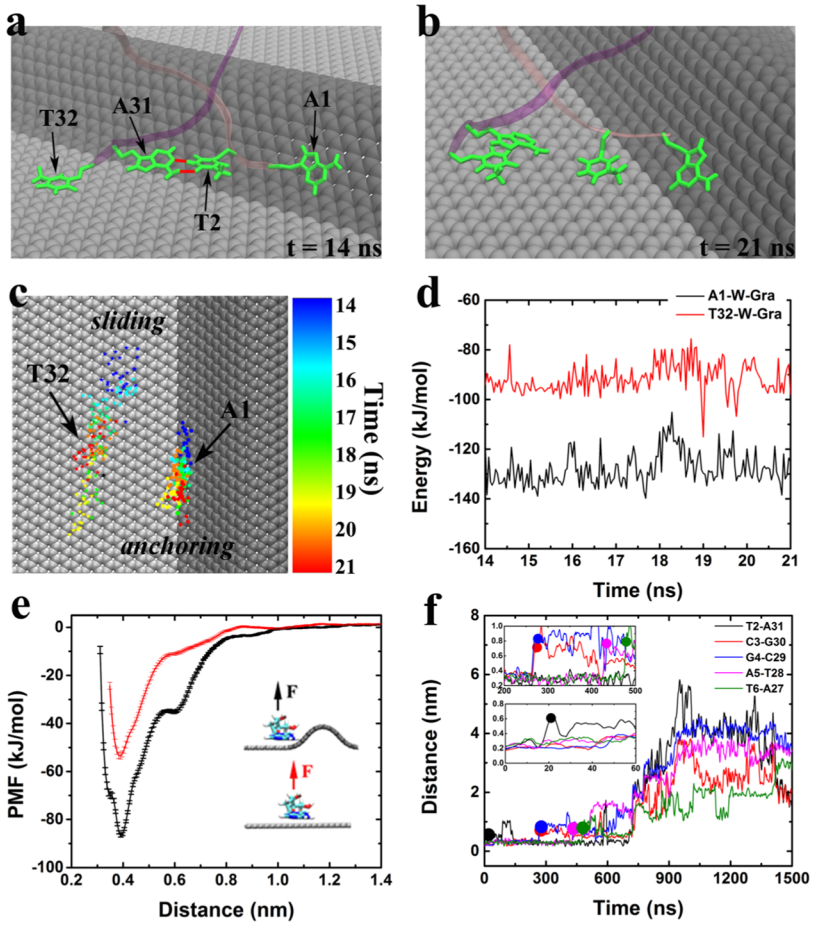

Figure 5. (a, b) Representative snapshots showing the unfolding process of dsDNA on W-Gra. The hydrogen bonds between the terminal base pairs are shown as red lines. (c) Migration track map of bases A1 and T32 on the surface of W-Gra for t from 14 to 21 ns. (d) vdW interaction energy of bases A1 and T32 with W-Gra for *t* from 14 to 21 ns. (e) Binding free energy of adenine to the wrinkled (black) and planar (red) areas of graphene. (f) Time evolution of the distances between hydrogen-bonding atoms in the base pairs. Only distances for the first five base pairs are shown here. Elongation of the distance indicates the disruption of a base pair and the time of the disruption is indicated by a colored dot. The zoomed-in time series is shown as insets.

38 water molecules around it, as shown in Figure S3a. When base A1 adsorbed onto the graphene planar area, it formed the $\pi-\pi$ stacking with graphene and resulted in a loss of ∼17 interfacial water molecules (Figure S3b,d). While for base A1 contacted the graphene wrinkled area, as shown in Figure S3c,d, it lost ∼11 interfacial water molecules. This nanoscale dewetting can provide a strong hydrophobic driving force for the binding of bases in dsDNA.

The morphology of the wrinkles in W-Gra has some similarity in spirit to a carbon nanotube (CNT). It is thus intuitive to expect a similar denaturation capability to dsDNA from a CNT. Following the same protocols, we conducted three independent simulations to investigate the interaction of dsDNA with a CNT (with a diameter of ∼2.0 nm) and our results are summarized in Figure S4. Panels a−c display the final configurations of dsDNA bound onto the CNT. One can see that the dsDNA consistently exhibits a strong preference of an upright orientation relative to the CNT, which is similar to the binding patterns of dsDNA on the I-Gra. A similar analysis of the contact number, RMSD, and the hydrogen bonds ratio was performed (Figure S4d−f), all of which indicate a stable dsDNA upon binding to a CNT. Essentially, we observed detrimental dsDNA unfolding only when the dsDNA bound to wrinkled graphene but not idealized graphene or CNT, suggesting that it is the curvature heterogeneity in wrinkled graphene that causes the denaturation of dsDNA.

To further elucidate the unfolding mechanism of dsDNA on W-Gra, we examined in detail the initial steps in the unfolding process (14−21 ns) observed in one of the trajectories, during which the second base pair T2−A31 broke (the first base pair A1-T32 is unstable even in the I-Gra system). As shown in Figure 5a, by *t* = 14 ns, bases A1 and T32 have been adsorbed onto the wrinkled and the planar area of the nanosheet, respectively. At this time, the base T2 kept interacting with the base A31 through two hydrogen bonds. About 7 ns later, these two hydrogen bonds broke, resulting in the exposure of T2 and A31, which immediately formed stable contacts with W-Gra (Figure 5b). Note that, during this process, base A1 only moved along the edge of the wrinkle, while base T32 could slide relatively freely on the planar area of the W-Gra surface, as shown in Figure 5c. The free movement of the T32-chain created a "centripetal force" relative to the restrained A1-chain, tearing the second base pair apart.

This special movement pattern can be attributed to the energy difference for binding to different parts of W-Gra with curvature heterogeneity. We calculated the vdW interaction energy of bases A1 and T32 with W-Gra. As displayed in Figure 5d, the mean value of the vdW interaction energy

https://dx.doi.org/10.1021/acs.jpcc.9b08778
J. Phys. Chem. C 2020, 124, 3332−3340

between W-Gra and base A1 (−128 kJ/mol) is much stronger than that between W-Gra and base T32 (−91.7kJ/mol). It is clear that, energetically, the wrinkled area attracts deoxyribonucleic acids more than the planar area. To further validate this finding, we calculated the binding free energy of a single adenine (as model system) adsorbing onto the wrinkled and planar areas of graphene, respectively, using the umbrella sampling method (Figure 5e). The results indicate that the binding affinity of adenine with the wrinkled area is much stronger than that with the planar area (−86.7 vs −53.5 kJ/mol). The energy barrier for escaping from the wrinkled area to the planar area (33.2 kJ/mol) is high and improbable to cross at room temperature. Therefore, the movements of the bases that came into contact with W-Gra are highly restrained to the wrinkled area (especially along the edges of the wrinkle), causing them to act like anchors.

The morphology of nanomaterials leading to different adsorption capabilities was also found in our previous studies,[80,82] where the concave surface of graphene exhibited a stronger dispersion interaction with phospholipids[82] or peptides[80] than the convex surface due to a larger number of contacts that can be established. Similarly, the intersection between the wrinkled and planar areas resembles a local "concave surface", thus providing the strongest interaction with dsDNA.

Lastly, we analyzed the evolution of the distance between the atoms in base pairs that formed hydrogen bonds at the initial state. The results are summarized in Figure 5f. At t = 21 ns, the distance between bases T2 and A31 increased to 0.61 nm, suggesting the loss of the hydrogen bond between this base pair, as displayed in Figure 5b. The breakage of the hydrogen bonds between the third, fourth, fifth, and sixth base pairs (C3-G30, G4-C29, A5-T28, T6-A27) occurred at roughly 265, 267, 433, and 480 ns, respectively. The other two trajectories also showed a similar unfolding process in which the base pairs broke sequentially (Figures S5 and S6) and the entire strand unfolds like a slider opening up a zipper (i.e., "zipper-like unfolding").

Notably, the distance between bases T2 and A31 decreased back to ∼0.28 nm occasionally (Figure 5f) during the rest of the trajectory. This is due to the formation of stacking after the breakage of the hydrogen bonds (Figure S7a) or reforming of the broken hydrogen bond when it transferred to the planar area due to the relatively free sliding on the planar area (Figure S7b). However, the stacking or the reformed H-bond could not stop the unfolding, and the T2−A31 base pair eventually disappeared altogether with the unfolding of the entire dsDNA molecule.

To examine the reliability of our simulations and to rule out the possibility that unsuitable force field parameters might have caused the unfolding phenomenon, we have further simulated the adsorption of dsDNA on W-Gra using two more force fields, the CHARMM36 and AMBER03 force fields. The results are despicted in Figures S8 and S9, respectively. For the three independent simulation trajectories using the CHARMM36 force field, similar unfolding events were observed for the structure of dsDNA after adsorbing onto the W-Gra surface, as shown in Figure S8a−c. The interaction energies and contact numbers between the dsDNA and W-Gra values with CHARMM36 are similar to those with CHARMM27 (Figure S8d,e). The only slight differences are in the kinetics, which should be expected. The large RMSD values (Figure S8f) indicate that the structural integrity of dsDNA was destroyed after binding to the W-Gra surface. Figure S8g shows that ∼40 to ∼45% of the hydrogen bonds in dsDNA were lost after binding to the W-Gra surface for the CHARMM36 force field (30−70% loss in CHARMM27). The simulations using the AMBER03 force field and the related results are summarized in Figure S9. The AMBER03 force field also shows similar unfolding of the structure of dsDNA after adsorbing onto W-Gra. These results with two other force fields suggest that the denaturation of dsDNA on W-Gra was most likely not caused by the overall imbalance in the simulation force field but by the wrinkles in graphene.

Finally, to illustrate the wrinkle size effect on the denaturation process of dsDNA, we also conducted simulations between dsDNA and the W-Gra with a larger wrinkle size (abbreviated as LW-Gra). The data are summarized in the Supporting Information as Figure S10. Similar denaturation events were observed for the structure of dsDNA, with expected slight differences in the kinetics (Figure S10b,c). As shown in Figure S10d, the RMSD values of dsDNA heavy atoms relative to the crystal structure are stabilized well above 2 nm (vs 1.2−2.0 nm in W-Gra). This indicates that the structural integrity of dsDNA was destroyed after binding to the LW-Gra surface and the denatured structure binds on the surface well stably. Figure S10e shows that ∼ 80% of the hydrogen bonds in dsDNA were lost after binding to the LW-Gra surface (vs 30−70% loss in W-Gra). This is consistent with the fact that the dsDNA in the LW-Gra system lost its structural integrity, as shown in Figure S10a. As shown in Figure S10f, the dsDNA shows a similar zipper-like unfolding process in which the base pairs broke sequentially and the entire strand unfolded like a slider opening up a zipper.

CONCLUSIONS

In summary, the interaction between a dsDNA segment and a wrinkled graphene nanosheet was systematically investigated using molecular dynamics simulations. The simulation results demonstrate that dsDNA experiences severe structural deformation upon binding to the wrinkled graphene surface. In contrast, upon binding to an ideal planar graphene nanosheet, it remains standing upright on the graphene surface and maintains its native structure. The free energy profile calculated from umbrella sampling suggests that the binding affinity of dsDNA bases with the wrinkled area is stronger than that with the planar area. This energy difference restrains the motion of the bases in contact with W-Gra to the wrinkled area, which serves as the seed to the unfolding of dsDNA. The unfolding mechanism of dsDNA on W-Gra can be summarized as follows: (1) the terminal bases are attracted to the wrinkled area, where the strong attraction effectively restrains the movements of these bases, causing them to act as anchors. (2) The movements of other parts of the dsDNA create a centripetal stretching force around the anchoring bases, tearing apart the hydrogen bonds between the base pairs and leading to local denaturation. Such local denaturation displays a zipper-like unfolding, in which the disruption starts from the first base pair and spreads sequentially to the neighboring pairs. This zipper-like unfolding mechanism is consistently observed in our simulations and is likely a common phenomenon for wrinkle-assisted dsDNA denaturation. (3) The local unfolding releases more initially distant and untouching dsDNA bases to form contact with W-Gra, which in turn accelerates the unfolding of dsDNA. Our current findings highlight the importance of wrinkles in the interaction of nanomaterials with

https://dx.doi.org/10.1021/acs.jpcc.9b08778
J. Phys. Chem. C 2020, 124, 3332−3340

biomolecules at their nano−bio interface (with curvature heterogeneity), which not only helps deepen our understanding of nanotoxicity in general but also offers new insight for potential design of future bio−nano sensors.

■ ASSOCIATED CONTENT

Supporting Information

The Supporting Information is available free of charge at https://pubs.acs.org/doi/10.1021/acs.jpcc.9b08778.

Representative snapshots from trajectory 2 of the W-Gra system showing the adsorption process of dsDNA onto the W-Gra surface (Figure S1); representative snapshots from trajectory 3 of the W-Gra system showing the adsorption process of dsDNA onto the W-Gra surface (Figure S2); water molecules distributed around base A1 in bulk (Figure S3); final binding conformations of dsDNA onto a CNT surface and time evolution of the contact number, RMSD, and intact hydrogen bonds of dsDNA upon binding to CNT (Figure S4); representative snapshots from trajectory 2 showing the unfolding process of dsDNA (Figure S5); representative snapshots from trajectory3 showing the unfolding process of dsDNA (Figure S6); representative snapshots from trajectory 1 showing the formation of self stacking (Figure S7);additional simulation of the system with another force field CHARMM36 (Figure S8); additional simulation of the system withone more force field AMBER03 (Figure S8); and additional simulation of the system with a larger wrinkle (PDF)

■ AUTHOR INFORMATION

Corresponding Authors

Xuan-Yu Meng − *Institute of Quantitative Biology and Medicine, State Key Laboratory of Radiation Medicine and Protection, School of Radiation Medicine and Protection, Collaborative Innovation Center of Radiation Medicine of Jiangsu Higher Education Institutions, Soochow University, Suzhou 215123, China;* orcid.org/0000-0003-1644-6552; Email: xymeng@suda.edu.cn

Ruhong Zhou − *Institute of Quantitative Biology and Medicine, State Key Laboratory of Radiation Medicine and Protection, School of Radiation Medicine and Protection, Collaborative Innovation Center of Radiation Medicine of Jiangsu Higher Education Institutions, Soochow University, Suzhou 215123, China; Department of Chemistry, Columbia University, New York 10027, United States;* orcid.org/0000-0001-8624-5591; Phone: +1 914-945-3591; Email: ruhongz@us.ibm.com

Authors

Baoyu Li − *Institute of Quantitative Biology and Medicine, State Key Laboratory of Radiation Medicine and Protection, School of Radiation Medicine and Protection, Collaborative Innovation Center of Radiation Medicine of Jiangsu Higher Education Institutions, Soochow University, Suzhou 215123, China*

Yuanzhao Zhang − *Computational Biological Center, IBM Thomas J. Watson Research Center, Yorktown Heights, New York 10598, United States*

Complete contact information is available at: https://pubs.acs.org/10.1021/acs.jpcc.9b08778

Notes

The authors declare no competing financial interest.

■ ACKNOWLEDGMENTS

We would like to thank Tien Huynh, Weifeng Li, and Zaixing Yang for help with this manuscript. This work was supported by the National Natural Science Foundation of China (Grant 11574224), A Project Funded by the Priority Academic Program Development of Jiangsu Higher Education Institutions (PAPD), and Jiangsu Provincial Key Laboratory of Radiation Medicine and Protection. R.Z. acknowledges the support from the IBM Blue Gene Science Program (W125859, W1464125, and W1464164).

■ REFERENCES

(1) Geim, A. K. Graphene: Status and Prospects. *Science* **2009**, *324*, 1530−1534.

(2) Balandin, A. A.; Ghosh, S.; Bao, W. Z.; Calizo, I.; Teweldebrhan, D.; Miao, F.; Lau, C. N. Superior Thermal Conductivity of Single-Layer Graphene. *Nano Lett.* **2008**, *8*, 902−907.

(3) Latil, S.; Henrard, L. Charge Carriers in Few-Layer Graphene Films. *Phys. Rev. Lett.* **2006**, *97*, No. 036803.

(4) Rao, C. N. R.; Sood, A. K.; Subrahmanyam, K. S.; Govindaraj, A. Graphene: The New Two-Dimensional Nanomaterial. *Angew. Chem., Int. Ed.* **2009**, *48*, 7752−7777.

(5) Novoselov, K. S.; Geim, A. K.; Morozov, S. V.; Jiang, D.; Zhang, Y.; Dubonos, S. V.; Grigorieva, I. V.; Firsov, A. A. Electric Field Effect in Atomically Thin Carbon Films. *Science* **2004**, *306*, 666−669.

(6) Zhang, K.; Zhang, L. L.; Zhao, X. S.; Wu, J. S. Graphene/Polyaniline Nanofiber Composites as Supercapacitor Electrodes. *Chem. Mater.* **2010**, *22*, 1392−1401.

(7) Loh, K. P.; Bao, Q. L.; Eda, G.; Chhowalla, M. Graphene Oxide as a Chemically Tunable Platform for Optical Applications. *Nat.Chem.* **2010**, *2*, 1015−1024.

(8) Schedin, F.; Geim, A. K.; Morozov, S. V.; Hill, E. W.; Blake, P.; Katsnelson, M. I.; Novoselov, K. S. Detection of Individual Gas Molecules Adsorbed on Graphene. *Nat. Mater.* **2007**, *6*, 652−655.

(9) Wang, H. L.; Cui, L. F.; Yang, Y. A.; Casalongue, H. S.; Robinson, J. T.; Liang, Y. Y.; Cui, Y.; Dai, H. J. Mn3o4-Graphene Hybrid as a High-Capacity Anode Material for Lithium Ion Batteries. *J. Am. Chem. Soc.* **2010**, *132*, 13978−13980.

(10) Wang, H. L.; Liang, Y. Y.; Mirfakhrai, T.; Chen, Z.; Casalongue, H. S.; Dai, H. J. Advanced Asymmetrical Supercapacitors Based on Graphene Hybrid Materials. *Nano Res.* **2011**, *4*, 729−736.

(11) Wu, Z. S.; Ren, W. C.; Wen, L.; Gao, L. B.; Zhao, J. P.; Chen, Z. P.; Zhou, G. M.; Li, F.; Cheng, H. M. Graphene Anchored with Co3o4 Nanoparticles as Anode of Lithium Ion Batteries with Enhanced Reversible Capacity and Cyclic Performance. *ACS Nano* **2010**, *4*, 3187−3194.

(12) Yang, K.; Zhang, S. A.; Zhang, G. X.; Sun, X. M.; Lee, S. T.; Liu, Z. A. Graphene in Mice: Ultrahigh in Vivo Tumor Uptake and Efficient Photothermal Therapy. *Nano Lett.* **2010**, *10*, 3318−3323.

(13) Ni, Z. H.; Wang, Y. Y.; Yu, T.; Shen, Z. X. Raman Spectroscopy and Imaging of Graphene. *Nano Res.* **2008**, *1*, 273−291.

(14) Liu, J. Q.; Cui, L.; Losic, D. Graphene and Graphene Oxide as New Nanocarriers for Drug Delivery Applications. *Acta Biomater.* **2013**, *9*, 9243−9257.

(15) Pumera, M. Graphene in Biosensing. *Mater. Today* **2011**, *14*, 308−315.

(16) Robinson, J. T.; Tabakman, S. M.; Liang, Y. Y.; Wang, H. L.; Casalongue, H. S.; Vinh, D.; Dai, H. J. Ultrasmall Reduced Graphene Oxide with High near-Infrared Absorbance for Photothermal Therapy. *J. Am. Chem. Soc.* **2011**, *133*, 6825−6831.

(17) Liu, Z.; Robinson, J. T.; Sun, X. M.; Dai, H. J. PEGylated Nanographene Oxide for Delivery of Water-Insoluble Cancer Drugs. *J. Am. Chem. Soc.* **2008**, *130*, 10876−10877.

(18) Akhavan, O.; Ghaderi, E.; Rahighi, R. Toward Single-DNA Electrochemical Biosensing by Graphene Nanowalls. *ACS Nano* **2012**, *6*, 2904−2916.
(19) Jung, J. H.; Cheon, D. S.; Liu, F.; Lee, K. B.; Seo, T. S. A Graphene Oxide Based Immuno-Biosensor for Pathogen Detection. *Angew. Chem., Int. Ed.* **2010**, *49*, 5708−5711.
(20) Tang, L. A. L.; Wang, J. Z.; Loh, K. P. Graphene-Based Seldi Probe with Ultrahigh Extraction and Sensitivity for DNA Oligomer. *J. Am. Chem. Soc.* **2010**, *132*, 10976−10977.
(21) Zhu, L. M.; Luo, L. Q.; Wang, Z. X. DNA Electrochemical Biosensor Based on Thionine-Graphene Nanocomposite. *Biosens. Bioelectron.* **2012**, *35*, 507−511.
(22) Kolosnjaj, J.; Szwarc, H.; Moussa, F. Toxicity Studies of Carbon Nanotubes. In *Bio-Applications of Nanoparticles*; Springer: NY, 2007; Vol. *620*, pp 181−204.
(23) Porter, A. E.; Gass, M.; Muller, K.; Skepper, J. N.; Midgley, P. A.; Welland, M. Direct Imaging of Single-Walled Carbon Nanotubes in Cells. *Nat. Nanotechnol.* **2007**, *2*, 713−717.
(24) Poland, C. A.; Duffin, R.; Kinloch, I.; Maynard, A.; Wallace, W. A. H.; Seaton, A.; Stone, V.; Brown, S.; MacNee, W.; Donaldson, K. Carbon Nanotubes Introduced into the Abdominal Cavity of Mice Show Asbestos-Like Pathogenicity in a Pilot Study. *Nat. Nanotechnol.* **2008**, *3*, 423−428.
(25) Ma-Hock, L.; Treumann, S.; Strauss, V.; Brill, S.; Luizi, F.; Mertler, M.; Wiench, K.; Gamer, A. O.; van Ravenzwaay, B.; Landsiedel, R. Inhalation Toxicity of Multiwall Carbon Nanotubes in Rats Exposed for 3 Months. *Toxicol. Sci.* **2009**, *112*, 468−481.
(26) Mitchell, L. A.; Lauer, F. T.; Burchiel, S. W.; McDonald, J. D. Mechanisms for How Inhaled Multiwalled Carbon Nanotubes Suppress Systemic Immune Function in Mice. *Nat. Nanotechnol.* **2009**, *4*, 451−456.
(27) Tu, Y. S.; et al. Destructive Extraction of Phospholipids from Escherichia Coli Membranes by Graphene Nanosheets. *Nat. Nanotechnol.* **2013**, *8*, 594−601.
(28) Zhao, X. C. Self-Assembly of DNA Segments on Graphene and Carbon Nanotube Arrays in Aqueous Solution: A Molecular Simulation Study. *J. Phys. Chem. C* **2011**, *115*, 6181−6189.
(29) Luan, B. Q.; Huynh, T.; Zhao, L.; Zhou, R. H. Potential Toxicity of Graphene to Cell Functions Via Disrupting Protein-Protein Interactions. *ACS Nano* **2015**, *9*, 663−669.
(30) Chong, Y.; Ge, C. C.; Yang, Z. X.; Garate, J. A.; Gu, Z. L.; Weber, J. K.; Liu, J. J.; Zhou, R. H. Reduced Cytotoxicity of Graphene Nanosheets Mediated by Blood-Protein Coating. *ACS Nano* **2015**, *9*, 5713−5724.
(31) Gu, Z.; Zhao, L.; Ge, C.; Liu, S.; Fang, G.; Chen, S. S.; Yang, Z.; Zhou, R. Facet-Regulated Adhesion of Double-Stranded DNA on Palladium Surfaces. *Nanoscale* **2019**, *11*, 1827−1836.
(32) Gu, Z. L.; Zhao, L.; Liu, S. T.; Duan, G. X.; Perez-Aguilar, J. M.; Luo, J. D.; Li, W. F.; Zhou, R. H. Orientational Binding of DNA Guided by the C2n Template. *ACS Nano* **2017**, *11*, 3198−3206.
(33) Li, Q.; et al. RNA Nanopatterning on Graphene. *2D Mater.* **2018**, *5*, No. 031006.
(34) Lu, C.; Liu, Y. B.; Ying, Y. B.; Liu, J. W. Comparison of Mos2, Ws2, and Graphene Oxide for DNA Adsorption and Sensing. *Langmuir* **2017**, *33*, 630−637.
(35) Saikia, N.; Pandey, R. Polarity-Induced Surface Recognition and Self-Assembly of Noncanonical DNA Nucleobases on H-Bn Monolayer. *J. Phys. Chem. C* **2018**, *122*, 3915−3925.
(36) Aggarwal, A.; Bag, S.; Maiti, P. K. Remarkable Similarity of Force Induced dsRNA Conformational Changes to Stretched Dsdna and Their Detection Using Electrical Measurements. *Phys. Chem. Chem. Phys.* **2018**, *20*, 28920−28928.
(37) Engel, M. C.; Smith, D. M.; Jobst, M. A.; Sagutdinow, M.; Liedl, T.; Romano, F.; Rovigatti, L.; Louis, A. A.; Doye, J. P. K. Force-Induced Unravelling of DNA Origami. *ACS Nano* **2018**, *12*, 6734−6747.
(38) Cocco, S.; Monasson, R.; Marko, J. F. Force and Kinetic Barriers to Unzipping of the DNA Double Helix. *Proc. Natl. Acad. Sci. U.S.A.* **2001**, *98*, 8608−8613.
(39) Marin-Gonzalez, A.; Vilhena, J. G.; Perez, R.; Moreno-Herrero, F. Understanding the Mechanical Response of Double-Stranded DNA and Rna under Constant Stretching Forces Using All-Atom Molecular Dynamics. *Proc. Natl. Acad. Sci. U.S.A.* **2017**, *114*, 7049−7054.
(40) McCauley, M. J.; Shokri, L.; Rouzina, I.; Williams, M. C. Kinetics of DNA Force-Induced Melting. *Biophys. J.* **2009**, *96*, No. 344a.
(41) Shen, J. L.; et al. Humidity-Responsive Single-Nanoparticle-Layer Plasmonic Films. *Adv. Mater.* **2017**, *29*, No. 1606796.
(42) De Luna, P.; Mahshid, S. S.; Das, J.; Luan, B. Q.; Sargent, E. H.; Kelley, S. O.; Zhou, R. H. High-Curvature Nanostructuring Enhances Probe Display for Biomolecular Detection. *Nano Lett.* **2017**, *17*, 1289−1295.
(43) Kim, K. S.; Zhao, Y.; Jang, H.; Lee, S. Y.; Kim, J. M.; Kim, K. S.; Ahn, J. H.; Kim, P.; Choi, J. Y.; Hong, B. H. Large-Scale Pattern Growth of Graphene Films for Stretchable Transparent Electrodes. *Nature* **2009**, *457*, 706−710.
(44) Li, X. S.; et al. Large-Area Synthesis of High-Quality and Uniform Graphene Films on Copper Foils. *Science* **2009**, *324*, 1312−1314.
(45) Lui, C. H.; Liu, L.; Mak, K. F.; Flynn, G. W.; Heinz, T. F. Ultraflat Graphene. *Nature* **2009**, *462*, 339−341.
(46) Jung, S. Y.; Rutter, G. M.; Klimov, N. N.; Newell, D. B.; Calizo, I.; Walker, A. R. H.; Zhitenev, N. B.; Stroscio, J. A. Evolution of Microscopic Localization in Graphene in a Magnetic Field from Scattering Resonances to Quantum Dots. *Nat. Phys.* **2011**, *7*, 245−251.
(47) Kim, E. A.; Castro Neto, A. H. Graphene as an Electronic Membrane. *Europhys. Lett.* **2008**, *84*, No. 57007.
(48) Yan, W.; He, W. Y.; Chu, Z. D.; Liu, M. X.; Meng, L.; Dou, R. F.; Zhang, Y. F.; Liu, Z. F.; Nie, J. C.; He, L. Strain and Curvature Induced Evolution of Electronic Band Structures in Twisted Graphene Bilayer. *Nat. Commun.* **2013**, *4*, No. 109.
(49) Zang, J. F.; Ryu, S.; Pugno, N.; Wang, Q. M.; Tu, Q.; Buehler, M. J.; Zhao, X. H. Multifunctionality and Control of the Crumpling and Unfolding of Large-Area Graphene. *Nat. Mater.* **2013**, *12*, 321−325.
(50) Levy, N.; Burke, S. A.; Meaker, K. L.; Panlasigui, M.; Zettl, A.; Guinea, F.; Neto, A. H. C.; Crommie, M. F. Strain-Induced Pseudo-Magnetic Fields Greater Than 300 Tesla in Graphene Nanobubbles. *Science* **2010**, *329*, 544−547.
(51) Deng, S. K.; Berry, V. Wrinkled, Rippled and Crumpled Graphene: An Overview of Formation Mechanism, Electronic Properties, and Applications. *Mater. Today* **2016**, *19*, 197−212.
(52) Yu, T.; Greish, K.; McGill, L. D.; Ray, A.; Ghandehari, H. Influence of Geometry, Porosity, and Surface Characteristics of Silica Nanoparticles on Acute Toxicity: Their Vasculature Effect and Tolerance Threshold. *ACS Nano* **2012**, *6*, 2289−2301.
(53) Huang, X. L.; Li, L. L.; Liu, T. L.; Hao, N. J.; Liu, H. Y.; Chen, D.; Tang, F. Q. The Shape Effect of Mesoporous Silica Nanoparticles on Biodistribution, Clearance, and Biocompatibility in Vivo. *ACS Nano* **2011**, *5*, 5390−5399.
(54) Geng, Y.; Dalhaimer, P.; Cai, S. S.; Tsai, R.; Tewari, M.; Minko, T.; Discher, D. E. Shape Effects of Filaments Versus Spherical Particles in Flow and Drug Delivery. *Nat. Nanotechnol.* **2007**, *2*, 249−255.
(55) Zuo, G.; Kang, S. G.; Xiu, P.; Zhao, Y.; Zhou, R. Interactions between Proteins and Carbon-Based Nanoparticles: Exploring the Origin of Nanotoxicity at the Molecular Level. *Small* **2013**, *9*, 1546−1556.
(56) Gong, X. J.; Li, J. Y.; Lu, H. J.; Wan, R. Z.; Li, J. C.; Hu, J.; Fang, H. P. A Charge-Driven Molecular Water Pump. *Nat. Nanotechnol.* **2007**, *2*, 709−712.
(57) Hummer, G.; Rasaiah, J. C.; Noworyta, J. P. Water Conduction through the Hydrophobic Channel of a Carbon Nanotube. *Nature* **2001**, *414*, 188−190.
(58) MacKerell, A. D.; et al. All-Atom Empirical Potential for Molecular Modeling and Dynamics Studies of Proteins. *J. Phys. Chem. B* **1998**, *102*, 3586−3616.

https://dx.doi.org/10.1021/acs.jpcc.9b08778
J. Phys. Chem. C 2020, 124, 3332−3340

(59) Best, R. B.; Zhu, X.; Shim, J.; Lopes, P. E. M.; Mittal, J.; Feig, M.; MacKerell, A. D. Optimization of the Additive Charmm All-Atom Protein Force Field Targeting Improved Sampling of the Backbone Phi, Psi and Side-Chain Chi(1) and Chi(2) Dihedral Angles. *J. Chem. Theory Comput.* **2012**, *8*, 3257−3273.
(60) Duan, Y.; et al. A Point-Charge Force Field for Molecular Mechanics Simulations of Proteins Based on Condensed-Phase Quantum Mechanical Calculations. *J. Comput. Chem.* **2003**, *24*, 1999−2012.
(61) Fang, G.; Li, W. F.; Shen, X. M.; Perez-Aguilar, J. M.; Chong, Y.; Gao, X. F.; Chai, Z. F.; Chen, C. Y.; Ge, C. C.; Zhou, R. H. Differential Pd-Nanocrystal Facets Demonstrate Distinct Antibacterial Activity against Gram-Positive and Gram-Negative Bacteria. *Nat. Commun.* **2018**, *9*, No. 129.
(62) Stirnemann, G.; Kang, S. G.; Zhou, R. H.; Berne, B. J. How Force Unfolding Differs from Chemical Denaturation. *Proc. Natl. Acad. Sci. U.S.A.* **2014**, *111*, 3413−3418.
(63) Xia, Z.; Clark, P.; Huynh, T.; Loher, P.; Zhao, Y.; Chen, H. W.; Rigoutsos, I.; Zhou, R. H. Molecular Dynamics Simulations of Ago Silencing Complexes Reveal a Large Repertoire of Admissible 'Seed-Less' Targets. *Sci. Rep.* **2012**, *2*, No. 569.
(64) Das, P.; Li, J. Y.; Royyuru, A. K.; Zhou, R. H. Free Energy Simulations Reveal a Double Mutant Avian H5n1 Virus Hemagglutinin with Altered Receptor Binding Specificity. *J. Comput. Chem.* **2009**, *30*, 1654−1663.
(65) Jorgensen, W. L.; Chandrasekhar, J.; Madura, J. D.; Impey, R. W.; Klein, M. L. Comparison of Simple Potential Functions for Simulating Liquid Water. *J. Chem. Phys.* **1983**, *79*, 926−935.
(66) Hess, B.; Kutzner, C.; van der Spoel, D.; Lindahl, E. Gromacs 4: Algorithms for Highly Efficient, Load-Balanced, and Scalable Molecular Simulation. *J. Chem. Theory Comput.* **2008**, *4*, 435−447.
(67) Humphrey, W.; Dalke, A.; Schulten, K. Vmd: Visual Molecular Dynamics. *J. Mol. Graphics* **1996**, *14*, 33−38.
(68) Darden, T.; York, D.; Pedersen, L. Particle Mesh Ewald—an N.Log(N) Method for Ewald Sums in Large Systems. *J. Chem. Phys.* **1993**, *98*, 10089−10092.
(69) Essmann, U.; Perera, L.; Berkowitz, M. L.; Darden, T.; Lee, H.; Pedersen, L. G. A Smooth Particle Mesh Ewald Method. *J. Chem. Phys.* **1995**, *103*, 8577−8593.
(70) Hess, B.; Bekker, H.; Berendsen, H. J. C.; Fraaije, J. Lincs: A Linear Constraint Solver for Molecular Simulations. *J. Comput. Chem.* **1997**, *18*, 1463−1472.
(71) Bussi, G.; Donadio, D.; Parrinello, M. Canonical Sampling through Velocity Rescaling. *J. Chem. Phys.* **2007**, *126*, No. 014101.
(72) Berendsen, H. J. C.; Postma, J. P. M.; Vangunsteren, W. F.; Dinola, A.; Haak, J. R. Molecular-Dynamics with Coupling to an External Bath. *J. Chem. Phys.* **1984**, *81*, 3684−3690.
(73) Roux, B. The Calculation of the Potential of Mean Force Using Computer-Simulations. *Comput. Phys. Commun.* **1995**, *91*, 275−282.
(74) Kumar, S.; Rosenberg, J. M.; Bouzida, D.; Swendsen, R. H.; Kollman, P. A. Multidimensional Free-Energy Calculations Using the Weighted Histogram Analysis Method. *J. Comput. Chem.* **1995**, *16*, 1339−1350.
(75) Torrie, G. M.; Valleau, J. P. Non-Physical Sampling Distributions in Monte-Carlo Free-Energy Estimation—Umbrella Sampling. *J. Comput. Phys.* **1977**, *23*, 187−199.
(76) Hub, J. S.; de Groot, B. L.; van der Spoel, D. G_Wham-a Free Weighted Histogram Analysis Implementation Including Robust Error and Autocorrelation Estimates. *J. Chem. Theory Comput.* **2010**, *6*, 3713−3720.
(77) Li, B. Y.; Bell, D. R.; Gu, Z. L.; Li, W. F.; Zhou, R. H. Protein ww Domain Denaturation on Defective Graphene Reveals the Significance of Nanomaterial Defects in Nanotoxicity. *Carbon* **2019**, *146*, 257−264.
(78) Zuo, G. H.; Gu, W.; Fang, H. P.; Zhou, R. H. Carbon Nanotube Wins the Competitive Binding over Proline-Rich Motif Ligand on Sh3 Domain. *J. Phys. Chem. C* **2011**, *115*, 12322−12328.
(79) Das, P.; Kapoor, D.; Halloran, K. T.; Zhou, R. H.; Matthews, C. R. Interplay between Drying and Stability of a Tim Barrel Protein: A Combined Simulation-Experimental Study. *J. Am. Chem. Soc.* **2013**, *135*, 1882−1890.
(80) Yin, X.; Li, B.; Liu, S.; Gu, Z.; Zhou, B.; Yang, Z. Effect of the Surface Curvature on Amyloid-B Peptide Adsorption for Graphene. *RSC Adv.* **2019**, *9*, 10094−10099.
(81) Zhou, R. H.; Huang, X. H.; Margulis, C. J.; Berne, B. J. Hydrophobic Collapse in Multidomain Protein Folding. *Science* **2004**, *305*, 1605−1609.
(82) Luan, B. Q.; Huynh, T.; Zhou, R. H. Complete Wetting of Graphene by Biological Lipids. *Nanoscale* **2016**, *8*, 5750−5754.

https://dx.doi.org/10.1021/acs.jpcc.9b08778
J. Phys. Chem. C 2020, 124, 3332−3340